Structural snapshots along the reaction mechanism of the atypical poplar thioredoxin-like2.1.

Kamel Chibani, Frederick Saul, Claude Didierjean, Nicolas Rouhier, Ahmed Haouz

FEBS Letters

FEBS PRESS science publishing by scientists

Structural snapshots along the reaction mechanism of the atypical poplar thioredoxin-like2.1

Kamel Chibani[1,†], Frederick Saul[2], Claude Didierjean[3], Nicolas Rouhier[1] and Ahmed Haouz[2]

1 UMR 1136, Interactions Arbres-Microorganismes, Faculté des Sciences et Technologies, Université de Lorraine/INRA, Vandœuvre-lès-Nancy, France
2 Institut Pasteur, Plateforme de Cristallographie, CNRS-UMR 3528, Paris, France
3 Université de Lorraine, CNRS, CRM2, Nancy, France

Correspondence
K. Chibani, UMR 1136, Interactions Arbres-Microorganismes, Faculté des Sciences et Technologies, Université de Lorraine/INRA, 54500 Vandœuvre-lès-Nancy, France
Fax: +49 521 106 6039
Tel: +49 521 106 5590
E-mail: kamel.chibani@uni-bielefeld.de
and
A. Haouz, Plateforme de Cristallographie, CNRS-UMR 3528, Institut Pasteur, 25 rue Dr. Roux, F-75724 Paris, France
Fax: +33 1 40 61 38 14
Tel: +33 1 40 61 39 30
E-mail: ahmed.haouz@pasteur.fr

[†]Present address
Department of Biochemistry and Physiology of Plants, Faculty of Biology, University of Bielefeld, 33615 Bielefeld, Germany

(Received 21 December 2017, revised 31 January 2018, accepted 8 February 2018, available online 4 March 2018)

doi:10.1002/1873-3468.13009

Edited by Stuart Ferguson

Plastidial thioredoxin (TRX)-like2.1 proteins are atypical thioredoxins possessing a WCRKC active site signature and using glutathione for recycling. To obtain structural information supporting the peculiar catalytic mechanisms and target proteins of these TRXs, we solved the crystal structures of poplar TRX-like2.1 in oxidized and reduced states and of mutated variants. These structures share similar folding with TRXs exhibiting the canonical WCGPC signature. Moreover, the overall conformation is not altered by reduction of the catalytic disulfide bond or in a C45S/C67S variant that formed a disulfide-bridged dimer possibly mimicking reaction intermediates with target proteins. Modeling of the interaction of TRX-like2.1 with both NADPH- and ferredoxin-thioredoxin reductases (FTR) indicates that the presence of Arg43 and Lys44 residues likely precludes reduction by the plastidial FTR.

Keywords: atypical thioredoxin; crystal structure; disulfide exchange; glutathione; *Populus*

Thioredoxins (TRXs) are ubiquitous proteins present in most prokaryotes and eukaryotes, which catalyze dithiol-disulfide exchange reactions [1]. In plants, TRXs are classified according to their gene structure, primary structure, and subcellular localization. Various TRX types are present in chloroplasts/plastids, including TRX f, m, x, y, z, CDSP32, and several TRX-lilium and TRX-like proteins [2,3]. Thioredoxins of the o-type are located in mitochondria [4], while h-type TRXs are found in the cytosol, mitochondria, or attached to the plasma membrane or to the ER/Golgi endomembrane system [5–7]. These proteins share similar overall three-dimensional topology with proteins such as glutaredoxins (GRXs) and protein disulfide isomerases (PDIs), which often contain additional protein domains [8,9].

Abbreviations
FTR, ferredoxin-thioredoxin reductase; GSH, reduced glutathione; GSSG, oxidized glutathione; NTR, NADPH-thioredoxin reductase; TRX, thioredoxin.

The overall polypeptide chain fold of TRXs is highly conserved among species and consists of a central five-stranded β-sheet surrounded by four α-helices [10]. Typical TRXs possess a canonical WC[G/P]PC active site signature located in a highly conserved and exposed region [2]. Both active site cysteine residues are generally required for the reduction of disulfide bonds in target proteins [11]. The first (catalytic) cysteine performs a nucleophilic attack on the target disulfide bonds, leading to the formation of an intermolecular disulfide bond with the target protein. This mixed disulfide intermediate is then attacked by the second (resolving) cysteine, resulting in the release of a reduced target protein and an oxidized TRX. The subsequent reduction of TRXs depends on their subcellular localization; most cytosolic and mitochondrial TRXs are reduced by an NADPH-TRX reductase (NTR) [12]. In chloroplasts, this reduction is mediated by the ferredoxin-TRX reductase (FTR) with electrons provided by the photosynthetic electron transport chain [11,13]. A particular case is the plastidial NTRc, which is a fusion between NTR and TRX domains and thus relies on NADPH as the electron donor [14].

Some atypical TRX isoforms including TRX-like2.1 can use a glutathione (GSH)-dependent system for regeneration [15,16]. In the case of poplar TRX h4 and its plant orthologs, this recycling step involves an additional, conserved cysteine present at the fourth position from the N terminus and the reduction is mediated by a GSH/GRX system [17,18]. As the most abundant low molecular weight thiol in cells, GSH is essential for the regulation of cellular redox homeostasis [19]. In particular, GSH can modulate protein activity through glutathionylation, a reversible post-translational modification involving the formation of a disulfide bond between glutathione and free thiols of proteins [20]. Besides constituting a rapid switch for redox regulation, protein S-glutathionylation is part of the recycling mechanism of some thiol-dependent enzymes and may also be important for the protection of protein cysteines from irreversible oxidation [21]. The formation of glutathione adducts occurs either by reaction of an oxidized cysteine with GSH or by reaction of reduced cysteines with oxidized glutathione forms, the most common being disulfide glutathione (GSSG) and nitrosoglutathione (GSNO) [20]. Interestingly, some TRXs in various organisms can be glutathionylated at cysteine residues located outside the active site region. This modification impairs the reductase activity by interfering with the recycling system [22,23].

Genomic analyses of higher plant species have revealed the presence of a large number of TRX-like proteins, including TRX-like2.1, which possess a non-canonical WCRKC active site signature. TRX-like2.1 are present in most photosynthetic organisms, except in cyanobacteria and some algae such as *Chlamydomonas reinhardtii* [3]. Although many three-dimensional structures have been solved for both prokaryotic and eukaryotic TRXs with canonical WC[G/P]PC active sites, this is not the case for atypical TRXs. Since the two residues located between the active site cysteines are important determinants for the redox and biochemical properties of TRXs in general, and of TRX-like 2.1 in particular [16,24], it is clearly important to explore these specificities at the structural level. Indeed, we previously observed that poplar TRX-like2.1 exhibited GSH-dependent activity despite being reduced *in vitro* by NTR, but not FTR [16]. Moreover, mutation of the active site signature from WCRKC to WCGPC significantly altered the specificity toward target proteins [16]. Here, we have determined the crystal structures of poplar TRX-like2.1 in the reduced or oxidized states, and of variants exhibiting a WCGPC signature or possessing only the first (catalytic) cysteine. These structures show that the atypical TRX-like2.1 has the same overall folding as typical TRXs and that the cationic residues Arg43 and Lys44 in the catalytic site play an important role in substrate recognition, precluding interaction with FTR or certain target proteins.

Materials and methods

Site-directed mutagenesis and protein purification

The pET-3d expression plasmids containing the sequences encoding TRX-like2.1 or TRX-like2.1 C45S [16] were used to introduce the C67S mutation by PCR using two complementary mutagenic primers, forward 5′ AAAATCAAATT CTATT**C**CGCGGATGTCAACAAG 3′ and reverse 5′ CT TGTTGACATCCGCG**G**AATAGAATTTGATTTT 3′. The presence of the mutation was confirmed by DNA sequencing. The recombinant plasmids were expressed in the BL21 (DE3) pSBET *Escherichia coli* strain and the corresponding recombinant proteins were purified following the procedure used for TRX-like2.1 [16].

Crystallization, data collection, and refinement

Crystallization screening trials were performed using the vapor diffusion method with a MosquitoTM nanoliter-dispensing system (TTP Labtech, Hertfordshire, UK). Sitting drops were set up with 400 nL of a 1 : 1 mixture of protein and crystallization solutions (672 different commercially available conditions) equilibrated against 150 μL reservoir

in multiwell plates (Greiner Bio-One, Solingen, Germany). The crystallization plates were stored at 18 °C in a Rock-Imager (Formulatrix, Bedford, MA, USA) automated imaging system to monitor crystal growth. Manual optimization was performed in Linbro plates with the hanging-drop method by mixing 2 μL of protein with 2 μL of reservoir solution. The best crystals were obtained with the conditions shown in Table 1. For data collection, the crystals were flash-cooled in liquid nitrogen using a paratone-paraffin oil mixture (50%/50%) as a cryoprotectant. The X-ray diffraction data were collected on beamline PROXIMA-1 (Synchrotron SOLEIL, St Aubin, France) or beamline BM-14 (Synchrotron ESRF, Grenoble, France). The diffraction images were integrated with the program XDS [25] and crystallographic calculations were carried out with programs from the CCP4 program suite [26]. The structure of TRX-like2.1 was solved by molecular replacement with the program PHASER [27] using TRX h1 from *C. reinhardtii* (PDB 1EP7) as a search model. The other structures were solved using TRX-like2.1 as a template. The structures were refined by alternate cycles of refinement with the program BUSTER [28,29] and manual adjustments were made to the models with COOT [30]. The crystallization conditions, crystal parameters, data statistics, and refinement parameters are shown in Table 1. All structural figures were generated with PYMOL (v 1.8.1.0, Schrödinger, LLC, New York, NY, USA). Structure analyses were done using the program CHIMERA (structure superimpositions) [31], the server PDB2PQR and the program APBS (electrostatic potential visualizations) [32], and the server EBI-PISA (exploration of protein interfaces) [33].

Assessing the reduction of oxidized TRX-like2.1 forms

The reduction of the TRX-like2.1 C45S/C67S dimer was monitored on nonreducing SDS/PAGE after incubating 15 μg of protein at room temperature for 15 min with 100 μM dithiothreitol (DTT), either reduced or oxidized, 500 μM GSH or a complete regeneration system mimicking physiological conditions and composed of either 20 μM NADPH/1 μM glutathione reductase (GR)/20 μM GSH or 20 μM NADPH/1 μM NTRB from *Arabidopsis thaliana* or 20 μM NADPH/40 nM ferredoxin (FDX)-NADP reductase (FNR)/1 μM FDX/1 μM FTR. NADPH, GR from Baker's yeast and GSH were obtained from SIGMA (Saint-Louis, MI, USA). Other proteins, *A. thaliana* NTRB, *C. reinhardtii* FNR, *Synechocystis* FDX and FTR, are recombinant proteins purified as described previously [34].

PDB accession numbers

The atomic coordinates and structure factors for TRX-like2.1 and its variants have been deposited in the RCSB Protein Data Bank with the pdb codes 5NYK, 5NYL, 5NYM, 5NYN, 5NYO, respectively, for oxidized TRX-like2.1, the WCGPC variant, reduced TRX-like2.1, TRX-like2.1 treated with GSSG, and the TRX-like2.1 C45S/C67S variant.

Results and Discussion

The oxidized and reduced forms of TRX-like2.1 are globally similar

A purified recombinant TRX-like2.1 in the oxidized state was first used for crystallographic analysis. The crystal belonged to space group $P2_12_12_1$ with a single molecule in the asymmetric unit and the structure was refined at 1.05 Å resolution (Table 1). The polypeptide chain could be traced from residues 5–122, with weak density for residues Gly104 and His105 suggesting mobility or disorder in this segment. The overall structure comprises five mixed β-strands surrounded by four α-helices in β1, α1, β2, α2, β3, α3, β4, β5, and α4 topology. The catalytic cysteine residues (Cys42 and Cys45) form a disulfide bond. Cys42 is located in an exposed loop between strand β2 and helix α2, while Cys45 is in helix α2 (Fig. 1A). An additional surface exposed cysteine residue (Cys67) is located in strand β3 near the catalytic site (Fig. 1A). TRX-like2.1 shares the same topological fold of typical TRXs such as *Homo sapiens* TRX1 (PDB 1ERU), *E. coli* Trx1 (PDB 2TRX), and *C. reinhardtii* TRX h1 (PDB 1EP7). The latter was used as the molecular replacement template model (Fig. 1B and Fig. S1). The overall RMSD in Cα positions of the superimposed structures is 1.3 Å (101 residues) despite the low sequence identities (Table S1). The conformation of the polypeptide chain in the active site region is similar in all structures. Most of the residues that play important catalytic and structural roles in canonical TRXs are conserved in TRX-like2.1 (Fig. S2) [35]. The most obvious feature of TRX-like2.1 is located between the two catalytic residues where the ^{43}RK^{44} sequence replaces the canonical GP sequence. Both of these charged hydrophilic side chains are exposed to solvent and make no specific intramolecular interactions. This ^{43}RK^{44} sequence plus the adjacent ^{104}HK^{105} sequence of the β5-α4 loop create a positive patch at the surface of the active site. In addition, the N-terminal end of helix α4 is elongated by one turn compared to *H. sapiens* TRX1, *E. coli* TRX1, and *C. reinhardtii* TRX h1. These properties lead to substantial differences in the surface and the electrostatic potential compared to other TRXs (Fig. S1).

To determine the structure of the catalytically active reduced form, crystals of TRX-like2.1 were soaked

Table 1. Crystallization conditions, data collection, and refinement statistics.

Crystal	Wild-type	WCGPC active site	Wild-type + DTT	Wild-type + GSSG	C45S/C67S variant
PDB ID	5NYK	5NYL	5NYM	5NYN	5NYO
Reservoir solution	0.2 M NaH_2PO_4	0.1 M Na_3 citrate	0.1 M Na acetate	0.1 M Na acetate	0.2 M Na formate
	1.6 M K_2HPO_4	20% (w/v) 2-propanol	0.2 M lithium sulfate	0.2 M lithium sulfate	20% (w/v) poly(ethylene glycol) 3350
	0.2 M NaCl	20% (w/v) poly(ethylene glycol) 4K	0.1 M hepes pH 7.5	0.1 M hepes pH 7.5	
	0.1 M imidazole, pH 8		25% (w/v) poly(ethylene glycol) 4K	25% (w/v) poly(ethylene glycol) 4K	
Protein concentration, $mg{\cdot}mL^{-1}$	4.8	14	4.8	4.8	2.7
Data collection					
Synchrotron beamline	SOLEIL Proxima 1	ESRF BM14	SOLEIL Proxima 1	SOLEIL Proxima 1	SOLEIL Proxima 1
Space group	$P2_12_12_1$	c2	$P2_12_12_1$	$P2_12_12_1$	$P4_12_12$
Unit cell dimensions, Å	a = 46.7, b = 52.86, c = 59.08	a = 57.65, b = 36.30, c = 100.20 (β = 91.1°)	a = 46.55, b = 52.95, c = 59.15	a = 46.71, b = 52.15, c = 59.78	$a = b$ = 62.55, c = 138.40
Resolution, Å	39.4–1.05 (1.07–1.05)	33.4–1.50 (1.53–1.50)	39.5–1.40 (1.42–1.40)	46.7–1.60 (1.63–1.60)	46.4–2.25 (2.32–2.25)
R_{merge}	0.069 (0.731)	0.042 (0.431)	0.021 (0.555)	0.057 (0.763)	0.068 (1.078)
R_{pim}	0.028 (0.295)	0.039 (0.410)	0.020 (0.512)	0.039 (0.548)	0.035 (0.552)
Unique reflections	66 294 (3045)	32 801 (1377)	28 141 (1268)	19 810 (984)	13 773 (1242)
$<I/s(I)>$	19.4 (3.4)	14.5 (2.0)	22.1 (2.0)	15.4 (2.0)	14.9 (2.1)
Mn(I) half-set correlation	0.999 (0.883)	0.999 (0.719)	1.000 (0.800)	0.999 (0.694)	0.998 (0.745)
Completeness, %	95.6 (89.9)	98.0 (83.8)	95.4 (87.9)	99.5 (100.0)	100.0 (100.0)
Multiplicity	13.5 (13.2)	3.4 (2.3)	3.6 (3.4)	5.6 (5.3)	8.5 (8.8)
Refinement					
Resolution, Å	15.4–1.05 (1.08–1.05)	33.4–1.50 (1.55–1.50)	39.5–1.40 (1.45–1.40)	16.4–1.60 (1.69–1.60)	46.4–2.25 (2.43–2.25)
No. of reflections	65 284 (4141)	32 797 (2652)	27 617 (2574)	19 506 (2614)	13 714 (2748)
R value, working set	0.1547 (0.1922)	0.1784 (0.2183)	0.1832 (0.2185)	0.1646 (0.1902)	0.2069 (0.2534)
R_{free}	0.1622 (0.1998)	0.2083 (0.2641)	0.2448 (0.3029)	0.1917 (0.2183)	0.2684 (0.2598)
Non-hydrogen protein atoms	973	1860	964	986	1938
No. of waters	300	224	202	173	98
rms deviations from ideal					
Bond length, Å	0.010	0.010	0.010	0.010	0.010
Bond angles, °	1.05	1.07	1.03	1.05	1.12
Ramachandran plot, %					
Preferred regions	99.1	97.8	98.3	99.1	97.4
Allowed regions	0.9	2.2	1.7	0.9	2.2
Outliers	0	0	0	0	0.4

Values in parentheses are for the highest resolution shell.

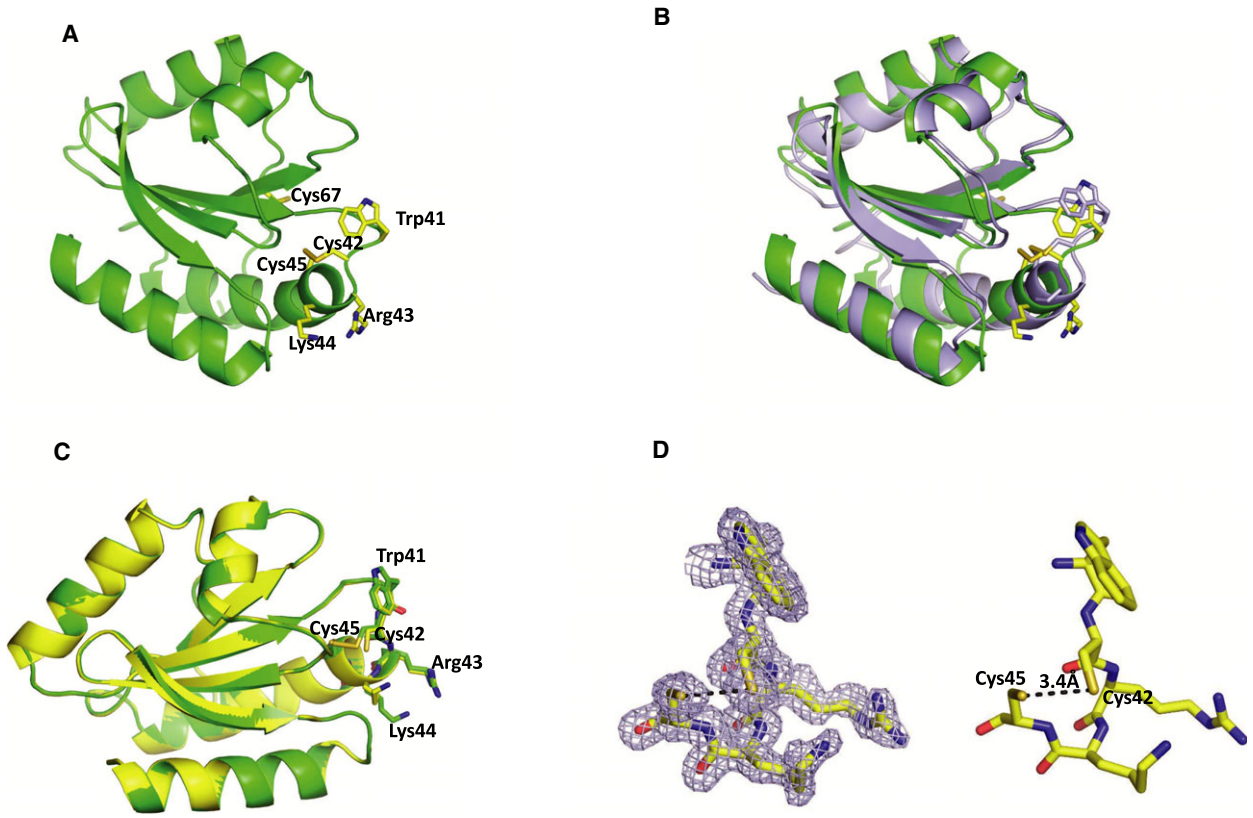

Fig. 1. Overall structures of the oxidized and reduced forms of poplar TRX-like2.1. (A) Three-dimensional structure of oxidized TRX-like2.1 with a detailed view of the WCRKC active site signature and the additional cysteine residue Cys67. (B) Oxidized TRX-like2.1 (green) is superimposed with *Chlamydomonas reinhardtii* TRX h1 (PDB entry 1EP7; gray). (C) Overall view of superimposition of reduced and oxidized TRX-like2.1 (in yellow and green, respectively). (D) 2Fo-Fc electron density map contoured at 1.0σ and structural model showing the disruption of the disulfide bond between catalytic cysteines in the reduced form of poplar TRX-like2.1.

overnight with 20 mM DTT and the corresponding structure was solved at 1.4 Å resolution (Table 1, Fig. 1C). Analysis of the crystal structure confirmed the reduction of the catalytic disulfide bond. The thiol groups of Cys42 and Cys45 are separated by 3.4 Å and are not engaged in any new covalent interactions (Fig. 1D). Comparison of the reduced and oxidized structures revealed only minor differences with an overall RMSD in Cα positions of 0.14 Å. The only other significant conformational difference in the active site region is a shift in the exposed side chain of Lys44 (Fig. 1C).

The absence of major structural variations between the oxidized and reduced forms of TRX-like2.1 is in agreement with observations made on human and *E. coli* TRXs for which the experimental structures of both forms were reported [36,37]. In human and *E. coli* TRXs, a displacement of the Trp residue in the WCGPC active site was observed. In human TRX, the reduction of the disulfide bond induces a shift of the indole ring leading to the removal of a hydrogen bond between Trp31-NE1 and Asp60-OD1. The equivalent Trp residue in TRX-like2.1 also exhibits a small shift without the hydrogen bond loss (Trp41-NE1 … OD1-Asn71). The hydrogen bond is also conserved in *E. coli* Trx1.

A covalent dimer is representative of an intermediate in the thiol-disulfide exchange reaction

The observations that TRX-like2.1 possesses a glutaredoxin activity profile, that the Cys42-Cys45 disulfide bond can be reduced by glutathione, and that the TRX-like2.1 C45S variant displays enzymatic activity comparable to the intact protein [16] suggested the existence of a glutathionylated intermediate on the catalytic cysteine. Cocrystallization and soaking experiments were performed with GSH or GSSG and the structure of TRX-like2.1 was solved at 1.7 Å

resolution with a crystal soaked overnight with 20 mM GSSG (Table 1). In this structure, a distance of 3.14 Å between the sulfhydryl groups of Cys42 and Cys45 indicated that the catalytic disulfide bond is predominantly reduced, but no glutathione was bound to one of these cysteine residues (Fig. 2A). Instead, a GSH is bound covalently to Cys67, but this adduct was only partially visible in the electron density (Fig. 2A,B). No hydrogen bond was observed between the GSH moiety and the protein, suggesting that there is no specific GSH-binding site. Although the role of the nonconserved Cys67 residue in TRX-like 2.1 is unclear, the binding of GSH suggests that it may be reactive. Indeed, it has been reported that glutathionylation of an additional cysteine (Cys60) in *A. thaliana* TRX f1 impaired its reduction by FTR, which selectively inactivates this isoform among other plastidial TRXs [23]. The human TRX1 possesses three additional cysteines that are involved in the formation of an intramolecular disulfide bond (Cys62-Cys69) and of an intermolecular disulfide (Cys73) and that can also be glutathionylated or nitrosylated [22,36,38,39]. These oxidized TRX forms could represent a means to inhibit TRX activity transiently under specific conditions. This could also be the case for poplar TRX-like2.1.

In order to obtain a glutathione adduct on the Cys42 of TRX-like2.1, we expressed and purified a C45S/C67S variant. This variant formed a covalent dimer in solution as observed in nonreducing SDS/PAGE (Fig. 3A). To determine whether this oxidized dimeric form could be reduced, the TRX-like2.1 C45S/C67S variant was incubated with DTT or GSH, with NADPH/GR/GSH (which ensured full reduction of GSH), with NADPH/NTR, and with NADPH/FNR/FDX/FTR (Fig. 3A). A treatment with oxidized DTT was performed to further oxidize the remaining monomeric form in solution. We observed that reduced DTT and GSH, but not the thioredoxin reductases, were able to fully reduce the homodimer (Fig. 3A). Crystallization trials were then performed with the untreated TRX-like2.1 C45S/C67S variant and with a prereduced variant treated with an excess of GSSG or GSNO to promote the glutathionylation of Cys42. However, we were only able to obtain crystals with the untreated protein (Table 1). The crystal structure of the C45S/C67S mutant confirmed the presence of a covalent disulfide bond between the catalytic Cys42 residues of two monomers (Fig. 3B). This dimeric structure likely mimics a covalent intermediate formed between TRXs and their protein targets in the first step of the enzymatic reaction. The overall folding topology of each monomer is maintained except in the vicinity of Cys42, where a significant rearrangement of the side-chain indole group of Trp41 is observed (Fig. 3C). In each monomer, the indole group of Trp41 makes hydrophobic interactions with Ile83 and Met86 of the second monomer. These observations are consistent with previous structural and functional studies suggesting that the conserved Trp41 plays an important role to maintain the active site in a bioactive conformation and to mediate protein target recognition during the catalytic reaction [40,41]. However, in other Trx-target structures, there is no significant conformational change of the equivalent tryptophan during complex formation (Fig. S3).

The TRX-like2.1 dimer interface of 550 $Å^2$ is roughly similar to those reported for other Trx-target complexes (Fig. S3). As found for the barley TRX h2-alpha-amylase/subtilisin inhibitor (BASI) complex, the loops β2-α2, α3-β4, and β5-α4 in TRXs are most often involved in the interaction with their target proteins

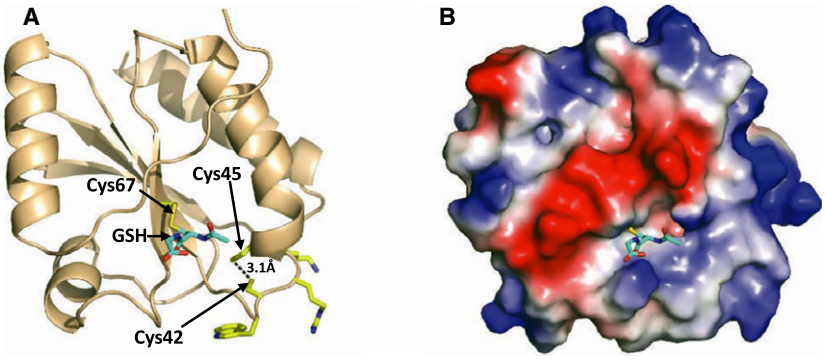

Fig. 2. GSH can bind to Cys67. (A) Ribbon diagram of TRX-like2.1 glutathionylated at Cys67 showing the reduction of the catalytic disulfide bond. (B) Protein electrostatic surface potential showing that the part of GSH observed in the electron density map is exposed to the solvent.

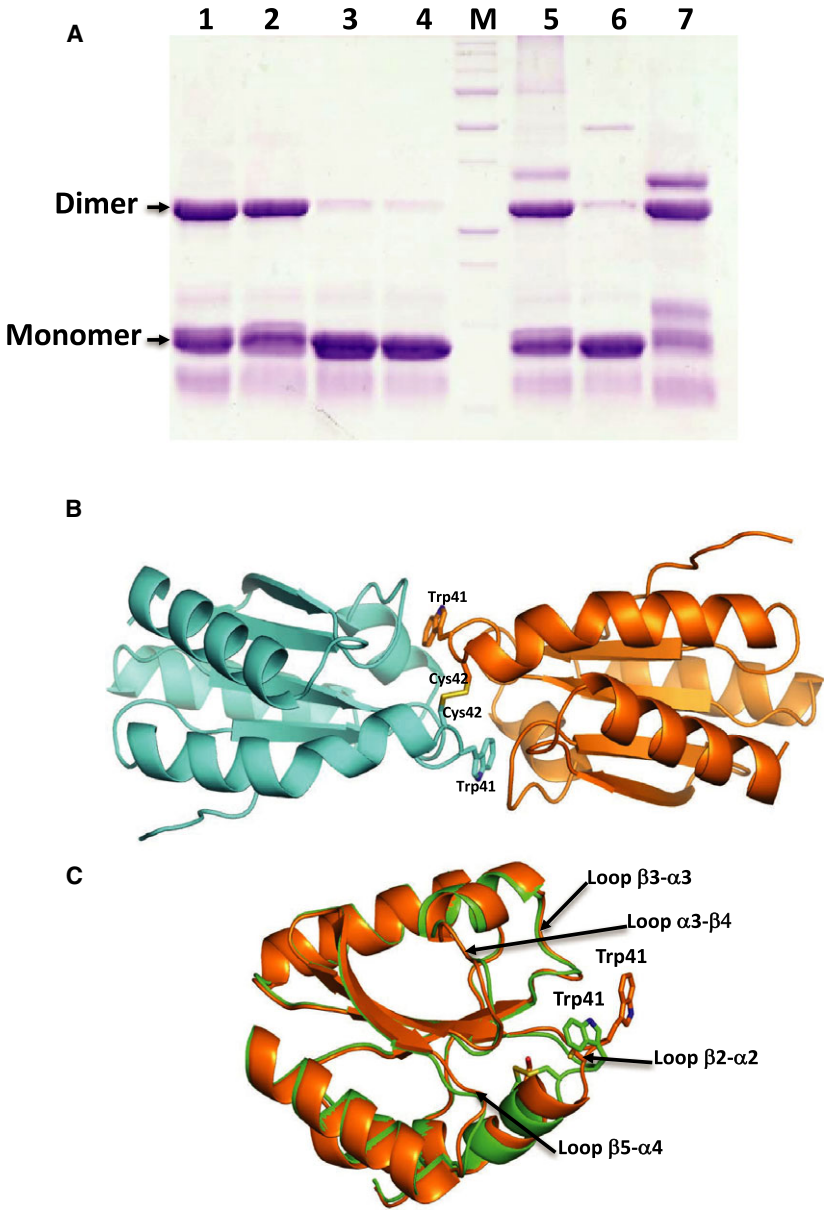

Fig. 3. Formation of a covalent homodimer in the C45S/C67S variant. (A) Nonreducing SDS/PAGE showing the reduction of an intermolecular disulfide in the C45S/C67S variant. The protein was either untreated (lane 1) or treated with 100 μM oxidized DTT (lane 2); with 500 μM reduced GSH (lane 3); with 100 μM reduced DTT (lane 4); with 20 μM NADPH + 1 μM AtNTRB (lane 5) with 20 μM NADPH + 1 μM GR + 100 μM GSH (lane 6), or with 20 μM NADPH + 40 nM FNR + 1 μM FDX + 1 μM FTR (lane 7). The lane M is the molecular weight marker. (B) Overall structure of the TRX-like2.1 C45S/C67S variant showing the covalent dimer formed between two monomers through the catalytic Cys42. (C) Superimposition of monomers of the oxidized TRX-like2.1 and of the C45S/C67S variant (in green and orange, respectively) showing the structural rearrangement of the side chain of Trp41 induced by the dimerization. The loops involved in interactions between monomers in the C45S/C67S covalent dimer are indicated by arrows.

[42]. The loops β2-α2 and α3-β4 are also engaged in TRX-like2.1 dimer stabilization mainly through hydrophobic interactions. In addition, the loop β3-α3 and the helix α3, located at the opposite side of the loop β5-α4 with respect to the central catalytic cysteine, also contribute to the interaction between TRX-like 2.1 monomers (Fig. 3C). Among the available crystal structures of TRX-target complexes, the only other example where these secondary structures participate in target recognition is that of the TlpA

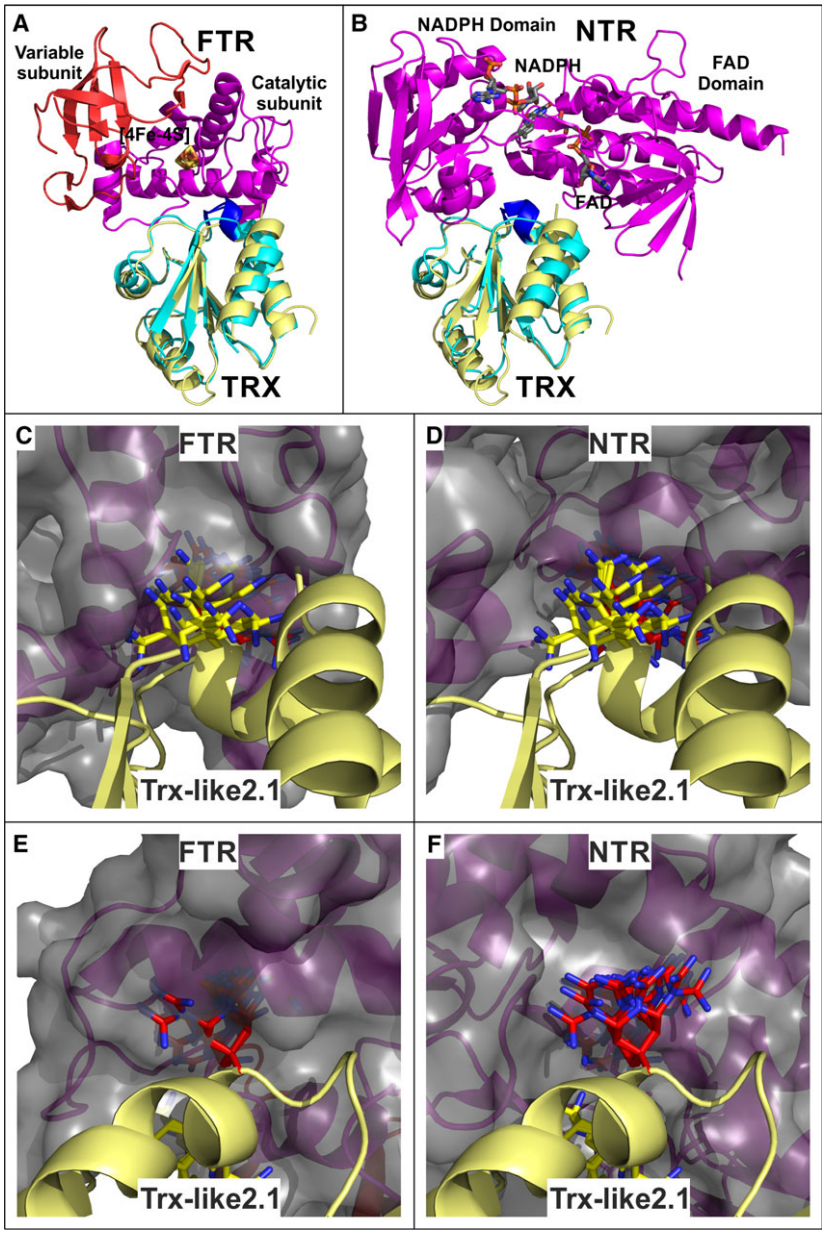

Fig. 4. Modeling of the interactions of poplar TRX-like2.1 with thioredoxin reductases. Superimposition of TRX-like2.1 (pale yellow) and TRX (cyan) from the FTR-TRX (PDB 1F6M) (A) and NTR-TRX (PDB 2PUK) (B) complexes. In both cases, the main chain of TRX-like2.1 active site residues closely overlaps with the active site residues of conventional TRX (blue). Side-chain conformational distributions of Lys44 (C, D) and Arg43 (E, F) of TRX-like2.1 in the generated 3D models. The rotamers were generated using COOT [30] from the backbone independent side-chain library of the Richardson group [49]. In the FTR-TRX-like2.1 complex (E), all Arg43 rotamers cross the Connolly surface of FTR indicating that no arginine rotamer is compatible with complex formation.

thioredoxin in complex with bacterial copper chaperone ScoI or with cytochrome oxidase subunit II [43]. Interestingly, TlpA displays some nonoverlapping surface areas for the recognition of both partners (Fig. S3). The shared overlap area involves residues from the loops β2-α2 and α3-β4 and the helix α3. These observations highlight the structural plasticity of TRXs to bind diverse protein substrates as underlined in a report describing a TRX from yeast in complex with a methionine sulfoxide reductase [44]. It is also worth noting that the subsequent dissociation of a complex between the oxidized TRX and a reduced target protein can be induced by conformational changes occurring at the level of the target, as reported in

the case of peroxiredoxins and methionine sulfoxide reductases [45,46].

The cationic residues of the TRX-like2.1 signature, Arg43 and Lys44, impact interactions with target proteins and notably hamper the reduction by FTR

We previously reported that a WCRKC to WCGPC conversion significantly altered the enzymatic activity profile of TRX-like 2.1, precluding the use of glutathione as a reductant while still allowing regeneration of a broader set of methionine sulfoxide reductases and peroxiredoxins [16]. To explore these differences further, the crystal structure of this WCGPC variant was solved (Table 1). The overall folding topology and active site architecture of the variant are similar to those of an intact TRX-like2.1 and of *C. reinhardtii* TRX h1, indicating that the exposed Arg43 and Lys44 are presumably sufficient to favor or prevent the recognition of specific target proteins. The reason why the WCGPC variant cannot be glutathionylated is unclear in light of this structure.

In order to understand why NTR, but not FTR, has the ability to reduce TRX-like2.1, we used the structural complexes of NTR-TRX (PDB entry 1F6M) and FTR-TRX (PDB entry 2PUK) as templates to model interactions with TRX-like2.1 [47,48]. In both complexes, the main chains of residues forming the WCRKC signature of TRX-like2.1 closely overlap with those of the conventional TRX active sites (Fig. 4A,B) but the side chains of Arg43 and Lys44 in the WCRKC active site clash due to steric hindrance with the reductases. In the NTR-TRX-like2.1 modeled complex, rotamers of the Arg43 and Lys44 side chains can be found that direct the positive charges to the solvent and preclude steric hindrance (Fig. 4C,E). However, in the FTR-TRX-like2.1 model, no arginine rotamer conformation was found compatible with complex formation (Fig. 4D,F). This likely explains why FTR is not able to reduce TRX-like2.1. In fact, an important difference between the structures of FTR and NTR is the localization of the cysteine residues involved in TRX reduction. In the case of NTR, these cysteines are located in a CXXC signature, whereas in FTR they are situated in two separate polypeptide loops, leading to increased constraints for the dithiol-disulfide exchange reaction. Hence, the presence of the arginine and lysine side chains adjacent to the two catalytic cysteines in TRX-like2.1 seems particularly important for interaction with partner proteins, both electron donors (reductases) and acceptors (targets). This adds an additional constraint to the local surface electrostatic potential, which is clearly a major factor in protein target recognition by TRXs, possibly more important than thermodynamic parameters such as the redox potentials of the respective protein partners.

Conclusions

We have determined the crystal structures of the atypical poplar TRX-like2.1 in oxidized and reduced states and a covalent complex with a glutathione adduct bound to an additional nonconserved Cys67. These structures share the same β1α1β2α2β3α3β4β5α4 topology as canonical TRXs despite the low sequence homology. The disulfide-bridged homodimeric structure obtained with the C45S/C67S variant may represent an intermediate state in the thiol-disulfide exchange reaction. This intermediate shows that no major conformational change would occur in TRX-like2.1 upon binding to the target protein, except for the catalytic Cys42 and adjacent Trp41 in the active site. Structural modeling with thioredoxin reductases supports previous biochemical observations that the two cationic residues (Arg43 and Lys44) in the active site signature of poplar TRX-like 2.1 prevent its recycling by FTR.

Acknowledgements

This work was supported by funding from the INRA-FORMAS program to KC and NR, and Institut Pasteur grants for AH and FS. We acknowledge synchrotrons SOLEIL and ESRF for provision of synchrotron radiation facilities and assistance. The authors are grateful to the staff of the crystallography platform at Institut Pasteur for robot-driven crystallization screening.

Author contributions

KC, NR and AH designed study. KC, FS, CD, NR and AH analyzed data. KC, AH drafted paper, and the final version was written through contribution of all authors.

References

1 Lemaire SD and Miginiac-Maslow M (2004) The thioredoxin superfamily in *Chlamydomonas reinhardtii*. *Photosynth Res* **82**, 203–220.
2 Meyer Y, Reichheld JP and Vignols F (2005) Thioredoxins in *Arabidopsis* and other plants. *Photosynth Res* **86**, 419–433.
3 Chibani K, Wingsle G, Jacquot JP, Gelhaye E and Rouhier N (2009) Comparative genomic study of the

thioredoxin family in photosynthetic organisms with emphasis on *Populus trichocarpa*. *Mol Plant* **2**, 308–322.
4 Laloi C, Rayapuram N, Chartier Y, Grienenberger JM, Bonnard G and Meyer Y (2001) Identification and characterization of a mitochondrial thioredoxin system in plants. *Proc Natl Acad Sci USA* **98**, 14144–14149.
5 Gelhaye E, Rouhier N, Gerard J, Jolivet Y, Gualberto J, Navrot N, Ohlsson PI, Wingsle G, Hirasawa M, Knaff DB *et al*. (2004) A specific form of thioredoxin h occurs in plant mitochondria and regulates the alternative oxidase. *Proc Natl Acad Sci USA* **101**, 14545–14550.
6 Renard M, Alkhalfioui F, Schmitt-Keichinger C, Ritzenthaler C and Montrichard F (2011) Identification and characterization of thioredoxin h isoforms differentially expressed in germinating seeds of the model legume *Medicago truncatula*. *Plant Physiol* **155**, 1113–1126.
7 Traverso JA, Micalella C, Martinez A, Brown SC, Satiat-Jeunemaître B, Meinnel T and Giglione C (2013) Roles of N-terminal fatty acid acylations in membrane compartment partitioning: *Arabidopsis* h-type thioredoxins as a case study. *Plant Cell* **25**, 1056–1077.
8 Rouhier N (2010) Plant glutaredoxins: pivotal players in redox biology and iron-sulphur centre assembly. *New Phytol* **186**, 365–372.
9 Selles B, Jacquot JP and Rouhier N (2011) Comparative genomic study of protein disulfide isomerases from photosynthetic organisms. *Genomics* **97**, 37–50.
10 Holmgren A, Söderberg BO, Eklund H and Brändén CI (1975) Three-dimensional structure of *Escherichia coli* thioredoxin-S2 to 2.8 Å resolution. *Proc Natl Acad Sci USA* **72**, 2305–2309.
11 Jacquot JP, Rouhier N and Gelhaye E (2002) Redox control by dithiol-disulfide exchange in plants: I. The chloroplastic systems. *Ann N Y Acad Sci* **973**, 508–519.
12 Rouhier N, Gelhaye E and Jacquot JP (2002) Redox control by dithiol-disulfide exchange in plants: II. The cytosolic and mitochondrial systems. *Ann N Y Acad Sci* **973**, 520–528.
13 Schürmann P and Jacquot JP (2000) Plant thioredoxin system revisited. *Annu Rev Plant Physiol Plant Mol Biol* **51**, 371–400.
14 Serrato AJ, Pérez-Ruiz JM, Spínola MC and Cejudo FJ (2004) A novel NADPH thioredoxin reductase, localized in the chloroplast, which deficiency causes hypersensitivity to abiotic stress in *Arabidopsis thaliana*. *J Biol Chem* **279**, 43821–43827.
15 Gelhaye E, Rouhier N and Jacquot JP (2003) Evidence for a subgroup of thioredoxin h that requires GSH/Grx for its reduction. *FEBS Lett* **555**, 443–448.
16 Chibani K, Tarrago L, Gualberto JM, Wingsle G, Rey P, Jacquot JP and Rouhier N (2012) Atypical thioredoxins in poplar: the glutathione-dependent thioredoxin-like 2.1 supports the activity of target enzymes possessing a single redox active cysteine. *Plant Physiol* **159**, 592–605.
17 Koh CS, Navrot N, Didierjean C, Rouhier N, Hirasawa M, Knaff DB, Wingsle G, Samian R, Jacquot JP, Corbier C *et al*. (2008) An atypical catalytic mechanism involving three cysteines of thioredoxin. *J Biol Chem* **283**, 23062–23072.
18 Meng L, Wong JH, Feldman LJ, Lemaux PG and Buchanan BB (2010) A membrane-associated thioredoxin required for plant growth moves from cell to cell, suggestive of a role in intercellular communication. *Proc Natl Acad Sci USA* **107**, 3900–3905.
19 Noctor G, Mhamdi A, Queval G, Chaouch S, Han Y, Neukermans J and Foyer CH (2011) Glutathione in plants: an integrated overview. *Plant, Cell Environ* **35**, 454–484.
20 Zaffagnini M, Bedhomme M, Marchand CH, Morisse S, Trost P and Lemaire SD (2012) Redox regulation in photosynthetic organisms: focus on glutathionylation. *Antioxid Redox Signal* **16**, 567–586.
21 Rouhier N, Lemaire SD and Jacquot JP (2008) The role of glutathione in photosynthetic organisms: emerging functions for glutaredoxins and glutathionylation. *Annu Rev Plant Biol* **59**, 143–166.
22 Casagrande S, Bonetto V, Fratelli M, Gianazza E, Eberini I, Massignan T, Salmona M, Chang G, Holmgren A and Ghezzi P (2002) Glutathionylation of human thioredoxin: a possible crosstalk between the glutathione and thioredoxin systems. *Proc Natl Acad Sci USA* **99**, 9745–9749.
23 Michelet L, Zaffagnini M, Marchand C, Collin V, Decottignies P, Tsan P, Lancelin JM, Trost P, Miginiac-Maslow M, Noctor G *et al*. (2005) Glutathionylation of chloroplast thioredoxin f is a redox signaling mechanism in plants. *Proc Natl Acad Sci USA* **102**, 16478–16483.
24 Chivers PT, Laboissière MC and Raines RT (1996) The CXXC motif: imperatives for the formation of native disulfide bonds in the cell. *EMBO J* **15**, 2659–2667.
25 Kabsch W (2010) Integration, scaling, space-group assignment and post-refinement. *Acta Crystallogr D Biol Crystallogr* **66**, 133–144.
26 Winn MD, Ballard CC, Cowtan KD, Dodson EJ, Emsley P, Evans PR, Keegan RM, Krissinel EB, Leslie AG, McCoy A *et al*. (2011) Overview of the CCP4 suite and current developments. *Acta Crystallogr D Biol Crystallogr* **67**, 235–242.
27 McCoy AJ, Grosse-Kunstleve RW, Adams PD, Winn MD, Storoni LC and Read RJ (2007) Phaser crystallographic software. *J Appl Crystallogr* **40**, 658–674.
28 Blanc E, Roversi P, Vonrhein C, Flensburg C, Lea SM and Bricogne G (2004) Refinement of severely incomplete structures with maximum likelihood in

BUSTER-TNT. *Acta Crystallogr D Biol Crystallogr* **60**, 2210–2221.
29 Smart OS, Womack TO, Flensburg C, Keller P, Paciorek W, Sharff A, Vonrhein C and Bricogne G (2012) Exploiting structure similarity in refinement: automated NCS and target-structure restraints in BUSTER. *Acta Crystallogr D Biol Crystallogr* **68**, 368–380.
30 Emsley P, Lohkamp B, Scott WG and Cowtan K (2010) Features and development of Coot. *Acta Crystallogr D Biol Crystallogr* **66**, 486–501.
31 Pettersen EF, Goddard TD, Huang CC, Couch GS, Greenblatt DM, Meng EC and Ferrin TE (2004) UCSF Chimera – a visualization system for exploratory research and analysis. *J Comput Chem* **25**, 1605–1612.
32 Jurrus E, Engel D, Star K, Monson K, Brandi J, Felberg LE, Brookes DH, Wilson L, Chen J, Liles K *et al.* (2018) Improvements to the APBS biomolecular solvation software suite. *Protein Sci* **27**, 112–128.
33 Krissinel E and Henrick K (2007) Inference of macromolecular assemblies from crystalline state. *J Mol Biol* **372**, 774–797.
34 Chibani K, Tarrago L, Schürmann P, Jacquot JP and Rouhier N (2011) Biochemical properties of poplar thioredoxin z. *FEBS Lett* **585**, 1077–1081.
35 Collet JF and Messens J (2010) Structure, function, and mechanism of thioredoxin proteins. *Antioxid Redox Signal* **13**, 1205–1216.
36 Weichsel A, Gasdaska JR, Powis G and Montfort WR (1996) Crystal structures of reduced, oxidized, and mutated human thioredoxins: evidence for a regulatory homodimer. *Structure* **4**, 35–51.
37 Jeng MF, Campbell AP, Begley T, Holmgren A, Case DA, Wright PE and Dyson HJ (1994) High-resolution solution structures of oxidized and reduced *Escherichia coli* thioredoxin. *Structure* **2**, 853–868.
38 Watson WH, Pohl J, Montfort WR, Stuchlik O, Reed MS, Powis G and Jones DP (2003) Redox potential of human thioredoxin 1 and identification of a second dithiol/disulfide motif. *J Biol Chem* **278**, 33408–33415.
39 Hashemy SI and Holmgren A (2008) Regulation of the catalytic activity and structure of human thioredoxin 1 via oxidation and S-nitrosylation of cysteine residues. *J Biol Chem* **283**, 21890–21898.
40 Menchise V, Corbier C, Didierjean C, Saviano M, Benedetti E, Jacquot JP and Aubry A (2001) Crystal structure of the wild-type and D30A mutant thioredoxin h of *Chlamydomonas reinhardtii* and implications for the catalytic mechanism. *Biochem J* **359**, 65–75.
41 Krause G and Holmgren A (1991) Substitution of the conserved tryptophan 31 in *Escherichia coli* thioredoxin by site-directed mutagenesis and structure-function analysis. *J Biol Chem* **266**, 4056–4066.
42 Maeda K, Hägglund P, Finnie C, Svensson B and Henriksen A (2006) Structural basis for target protein recognition by the protein disulfide reductase thioredoxin. *Structure* **14**, 1701–1710.
43 Abicht HK, Scharer MA, Quade N, Ledermann R, Mohorko E, Capitani G, Hennecke H and Glockshuber R (2014) How periplasmic thioredoxin TlpA reduces bacterial copper chaperone ScoI and cytochrome oxidase subunit II (CoxB) prior to metallation. *J Biol Chem* **289**, 32431–32444.
44 Ma XX, Guo PC, Shi WW, Luo M, Tan XF, Chen Y and Zhou CZ (2011) Structural plasticity of the thioredoxin recognition site of yeast methionine S-sulfoxide reductase Mxr1. *J Biol Chem* **286**, 13430–13437.
45 Rouhier N, Kauffmann B, Tete-Favier F, Palladino P, Gans P, Branlant G, Jacquot JP and Boschi-Muller S (2007) Functional and structural aspects of poplar cytosolic and plastidial type a methionine sulfoxide reductases. *J Biol Chem* **282**, 3367–3378.
46 Hall A, Nelson K, Poole LB and Karplus PA (2011) Structure-based insights into the catalytic power and conformational dexterity of peroxiredoxins. *Antioxid Redox Signal* **15**, 795–815.
47 Lennon BW, Williams CH and Ludwig ML (2000) Twists in catalysis: alternating conformations of *Escherichia coli* thioredoxin reductase. *Science* **289**, 1190–1194.
48 Dai S, Friemann R, Glauser DA, Bourquin F, Manieri W, Schürmann P and Eklund H (2007) Structural snapshots along the reaction pathway of ferredoxin–thioredoxin reductase. *Nature* **448**, 92–96.
49 Lovell SC, Word JM, Richardson JS and Richardson DC (2000) The penultimate rotamer library. *Proteins* **40**, 389–408.

Supporting information

Additional Supporting Information may be found online in the supporting information tab for this article:

Fig. S1. Superimpositions of poplar TRX-like2.1 (reduced form, light blue), *C. reinhardtii* TRX h1 (PDB 1EP7, magenta), *E. coli* Trx1 (PDB 2TRX, green), and *H. sapiens* TRX1 (PDB 1ERU, red), and electrostatic potential visualization of the corresponding TRXs.

Fig. S2. Sequence alignment of poplar TRX-like2.1 (UNP I0BZV0), *C. reinhardtii* TRX h1 (UNP P80028), *E. coli* Trx1 (UNP P0AA25), and *H. sapiens* TRX1 (UNP P10599).

Fig. S3. Crystal structures of TRX-like2.1 dimer and TRXs in a mixed disulfide complex with target proteins: HvTRXh2–BASI (thioredoxin h2 and alpha-amylase/subtilisin inhibitor from *Hordeum vulgare var. distichum*, PDB 2IWT), HsTRX–TXNIP (thioredoxin

and thioredoxin-interacting protein from *Homo sapiens*, PDB 4LL1), EcTRX–PAPSr (thioredoxin and 3′-phosphoadenosine-5′-phosphosulfate reductase from *Escherichia coli*, PDB 2O8V), ScTRX–PRX (homodimer) (thioredoxin Trx2 and peroxiredoxin Ahp1 from *Saccharomyces cerevisiae*, PDB 4DSS), ScTrx–Mxr1 (thioredoxin Trx2 and methionine S-sulfoxide reductase Mxr1 from *Saccharomyces cerevisiae*, PDB 3PIN), BdTRX–Cox (thioredoxin-like TlpAs and subunit II of cytochrome c oxidase CoxBPD from *Bradyrhizobium diazoefficiens*, PDB 4TXV), BdTRX–Scols (thioredoxin-like TlpAs and copper chaperone ScoIs from *Bradyrhizobium diazoefficiens*, PDB 4TXV).

Table S1. Homology/Identity percentages between the amino acid sequences of poplar TRX-like2.1 (UNP I0BZV0), *C. reinhardtii* TRX h1 (UNP P80028), *E. coli* Trx1 (UNP P0AA25), and *H. sapiens* TRX1 (UNP P10599).